A Laser-Processed Silicon Solar Cell with Photovoltaic Efficiency in the Infrared

Maria Isabel Sánchez,* Philippe Delaporte, Yohann Spiegel, Ben Franta, Eric Mazur, and Thierry Sarnet

Hyperdoped and textured silicon created with a femtosecond laser in the presence of SF_6 gas has a highly absorbing surface with extended spectral sensitivity in the infrared. The main drawback of this micro- and nanostructured material for photovoltaic (PV) cells is an increase in charge-carrier recombination at the surface due to the typically poor crystallinity of the surface layer. Laser annealing postprocessing of the black silicon (b-Si) surface is used to greatly reduce the crystal structure defects while maintaining sub-bandgap absorption. The back side of the cell is functionalized with spin-on doping and laser fired contacts to make an interdigitated back-contact proof-of-concept b-Si solar cell. It is shown that this cell has measurable PV efficiency in the sub-bandgap infrared, a promising step toward developing intermediate-band silicon PVs.

1. Introduction

For adopting fully renewable energy economy, photovoltaics (PVs) will play a major role. Increasing the power conversion efficiency (PCE) is of key importance as it reduces the amount of energy-intensive materials such as crystalline silicon (c-Si), hence reduces the energy payback.[1]

Nowadays, PV industry is mainly driven by c-Si solar cells; this is probably due to the standardization of technology in mass production and the rapid decrease in manufacturing cost (15% per year in average).[2] Despite the maturity of this technology, for almost 14 years, the highest PCE for c-Si solar cell stood at 25%. This c-Si solar cell had an area of 4 cm² and was based on the so-called passivated emitter and rear locally diffused (PERL)[3] solar-cell technology. In parallel with PERL cell, other

M. I. Sánchez, P. Delaporte, T. Sarnet
CNRS, LP3
Aix Marseille Université, UMR 7341
13288 Marseille, France
E-mail: sanchez@lp3.univ-mrs.fr

Y. Spiegel
Ion Beam, Services
ZI Peynier-Rousset
rue Gaston Imbert prolongée, Peynier 13790, France

B. Franta, E. Mazur
School of Engineering and Applied Sciences
Harvard University
29 Oxford Street, 225 Pierce Hall, Cambridge, MA 02138, USA

The ORCID identification number(s) for the author(s) of this article can be found under https://doi.org/10.1002/pssa.202000550.

high-efficiency cells structure was transferred to mass production, such as interdigitated back contact (IBC)[4] solar cell or heterojunction solar cells (SHJ).[5] Regardless of their high-efficiency potential, their market share is still limited.

The present efficiency record c-Si cell has a value of 26.7% (with an area of 79 cm²) and has a device structure that blends concepts from the SHJ and IBC cells.[4] The question now is whether new technological advances can further increase the efficiency of c- Si technology.

Recently, strategies toward broadening the spectral response[6] and further improve the PCE are possible with new multi-junction cell structures. Silicon-based tandem solar cells offer one of the most promising solutions for efficiencies above 28%. A potentially cheaper route is the use of perovskites[7] as top cells with current record efficiencies above 28%. In this case, long-term stability and low-cost mass production are still to be shown.

Further efficiency improvements addressed to enhance the spectral response are possible with new materials and luminescent processes which can modify the incident sunlight properties to better suit the cell optimal absorption regions.[8] This makes for an interesting area of research and promising techniques for enhancing the efficiency of solar cells, techniques such as upconversion (UC),[9,10] downconversion (DC),[11] luminescent downshifting (LDS),[12] or enhancing spectral modification via nanostructures[6,8] (Quantum dots, photonic crystals, core-shell nanostructures, plasmonic nanostructures have attracted extensive attention).

Figure 1 shows the AM 1.5 G solar spectrum and shows the spectral region where a standard perovskite solar cell effectively absorbs light, and the spectral regions where DS and UC can be utilized to reduce spectral losses. The yellow line region shows where DS can be used to convert high-energy photons to photons closer to the bandgap energy, thus minimalizing thermalization losses. The green line region shows where UC is required to enable absorption of photons whose energy is lower than silicon cells bandgap, crystalline (c-Si) ($Eg \approx 1.1$ eV) exhibit high spectral absorption in the visible/near infrared (NIR) region, with the efficiency decreasing gradually outside this window.

In addition to the previous strategies, the implementation of the namely black silicon (b-Si) was widely studied as potential solution to increase the efficiency by enhancing the spectral response of a solar cell.[13,14] Due to its high absorption in the
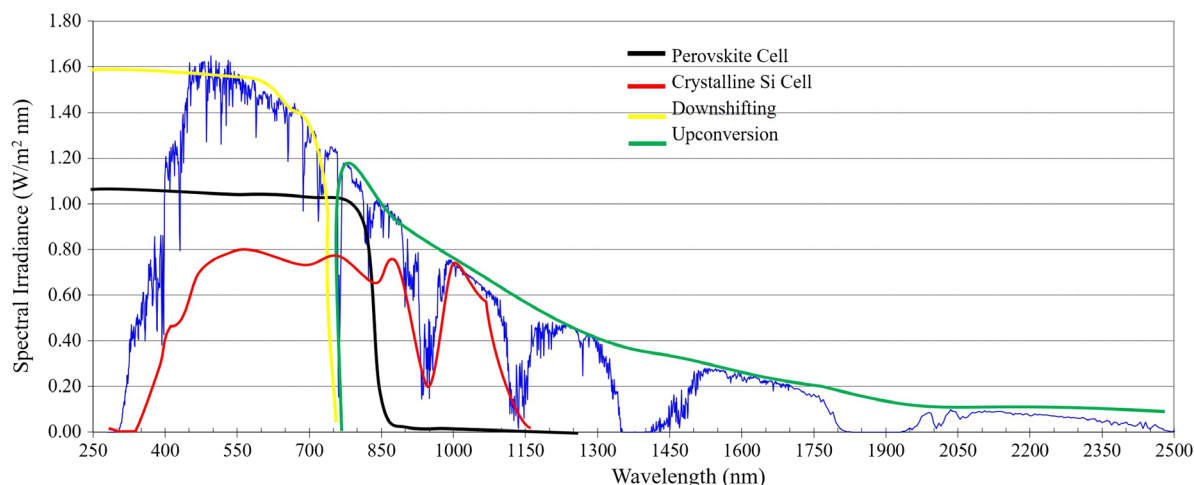
Figure 1. The spectral distribution of sunlight at air mass 1.5 global (solid blue line). As a guide for the eye is represented the fraction of incident radiation effectively harvested by a reference c-Si (red line), perovskite solar cell (dark blue), and the spectral regions in which downshifting (yellow) and UC (green) spectral converters can be exploited to improve the cell efficiency.

wide range from UV–visible to infrared, b-Si is extremely attractive for using as sensitive layer of photodiodes, photodetector, solar cells, field emission, luminescence, and other photoelectric devices. Intensive study has been performed to understand the enhanced absorption of b-Si as well as the response extended to infrared spectrum range.[15–18]

Very high absorptance values over the entire solar spectrum, including the infrared,[19,20] and at a wide range of incident angles can be achieved by hyperdoping and texturing silicon using femtosecond laser irradiation to create "black silicon" (b-Si).[20–25] Solar cells based on n-type b-Si substrates are of potential interest because, unlike p-type substrates, n-type b-Si does not exhibit light-induced degradation by the formation of boron–oxygen complexes, and it is less sensitive to the degradation of charge-carrier lifetime due to recombination through

active metal impurities.[26] **Figure 2** shows the measured absorption of our b-Si solar cell relative to AM-1.5 solar illumination.

In addition to its attractive optical properties, b-Si exhibits a large surface area and poor crystallinity in the surface skin layer, making carrier recombination in b-Si solar cells a critical issue. Recently, ns-laser annealing was reported to increase the crystallinity of the surface while retaining the high optical absorptance values.[27–35]

Within the framework presented earlier, this work addresses a novel IBC proof-of-concept b-Si solar cell, combining laser microprocessing for doping and metallization. Finally, it is presented as an electrical, physical–chemical, and PV characterizations of b-Si treated with ns-laser annealing. The final device leads to an improvement in efficiency at standard testing conditions (STC) by about 2%.
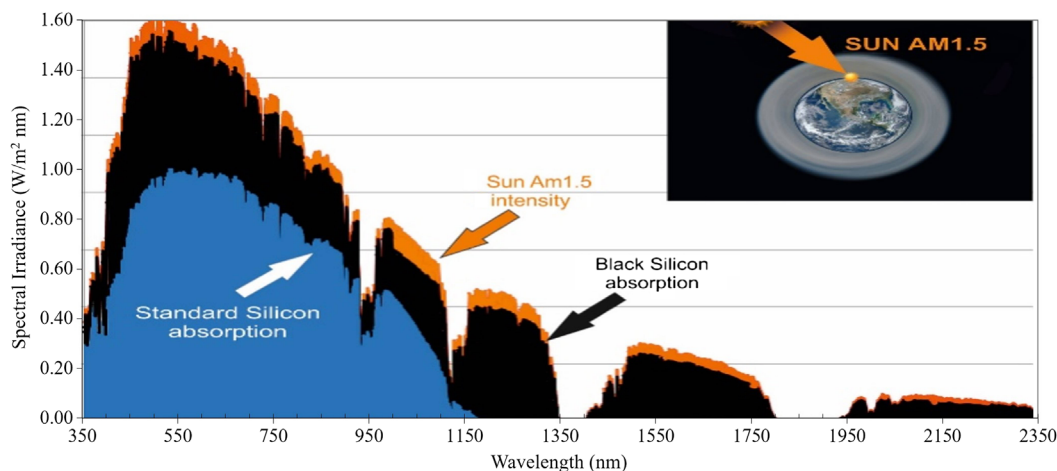
Figure 2. Experimental standard silicon and b-Si absorption versus solar illumination measured after solar radiation has traveled through the atmosphere (AM1.5). Globe image: Google Earth Data 2018 Data SIO, NOAA, USA. Navy, NGA, GEBCO, Image Landsat/Copernicus, Image IBCAO.

2. Experimental Section

b-Si was created on $2 \times 2 \, cm^2$ silicon wafers using femtosecond laser irradiation in the presence of sulfur hexafluoride (SF_6), as described in previous studies.[26–34,36] The wafers were n-type float-zone monocrystalline silicon with an <100> orientation, $5 \pm 0.2 - cm$ resistivity, and $200 \pm 15 \, \mu m$ thickness. The wafers were irradiated using a fs laser fluence of $5 \, kJ \, m^{-2}$ and 100 shots per area in an atmosphere of 100 Torr SF_6.

The b-Si was then treated with ns-laser annealing to heal the defects created by the fs laser treatment [37,38]. Nanosecond laser pulses were generated by an ArF excimer laser (193 nm) at 100 Hz and scanned across the b-Si surface (room temperature, ambient air at atmospheric pressure) at fluences of $0.5–1.5 \, J \, cm^{-2}$.

Before and after ns-laser annealing, we characterized the topography of the samples using scanning electron microscopy (SEM) and cross-sectional transmission electron microscopy (TEM). The crystallinity of the samples was also analyzed by electron diffraction and Raman spectroscopy. The optical absorptance was measured before and after ns-laser annealing using samples that underwent the same process without deposition of metal electrodes, which would interfere with the optical absorptance measurements.

Finally, small laboratory solar cells ($2 \times 2 \, cm^2$) were fabricated by adding IBCs[37] (**Figure 3**). To apply metal electrodes to the samples, we used a laser-fired contact (LFC) technique[37–39] by irradiating a 10 μm thick aluminum film with an ArF excimer laser (193 nm, 15 ns, 250 mJ@100 Hz), creating a metal–semiconductor alloy with ohmic behavior. This technique was developed by the Fraunhofer Institute for Solar Energy Systems (ISE)[40] and is a promising method for creating ohmic contacts in ambient conditions, while avoiding thermal evaporation or thermal annealing.
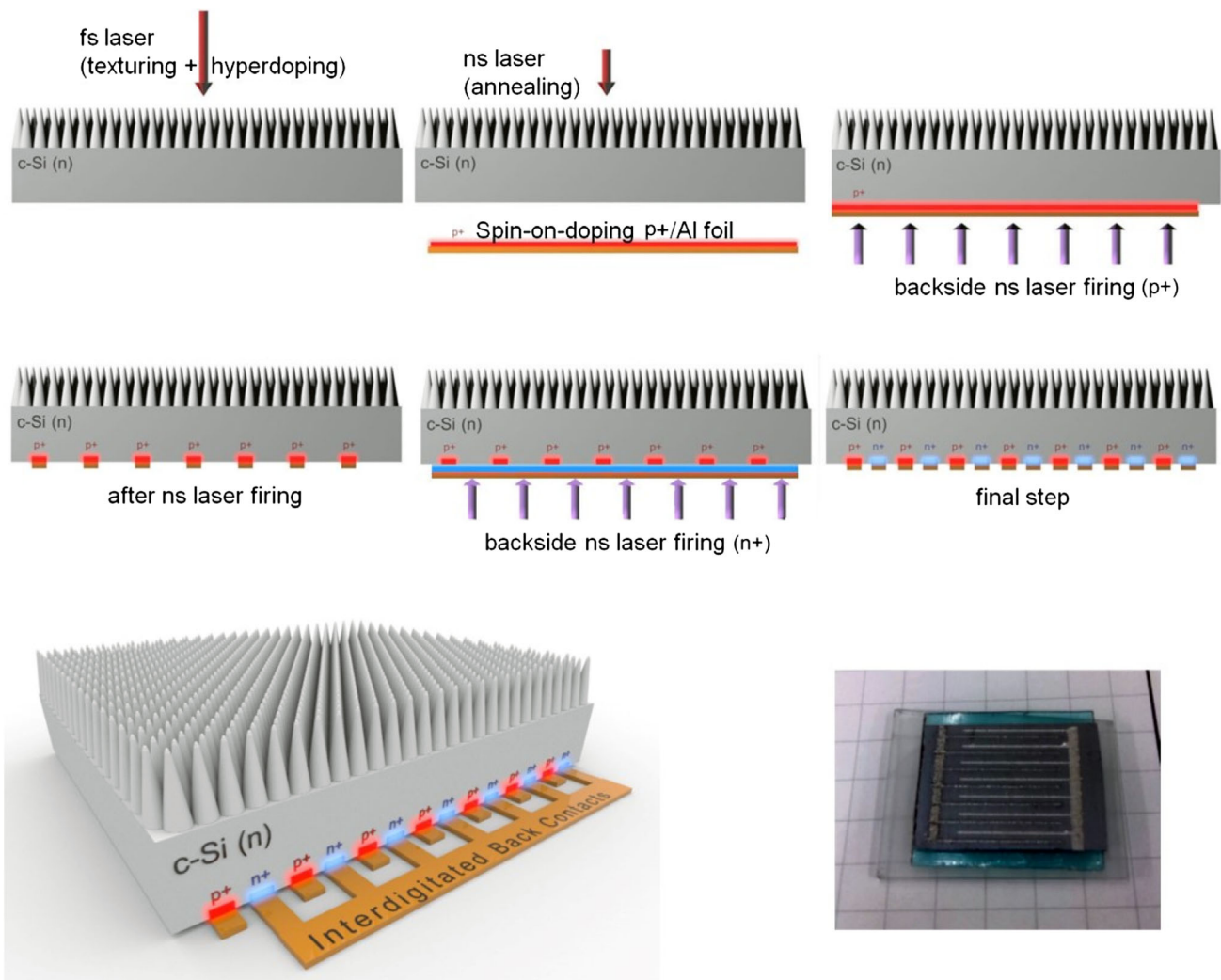

Figure 3. Top: Fabrication steps of the solar cell. Doping areas are created from spin-on-doping (SOD) deposition followed by Al foil deposition, and the contacts are made by laser irradiation.[25] Bottom left: Schematic picture of the final IBC structure (for clarity, the cell thickness is greatly exaggerated). Bottom right: Image of the IBC back-contact pattern in a final solar cell.

3. Results and Discussion

The SEM observations reveal that the hyperdoped b-Si surface exhibits the usual μm-scale conical structures (spikes)[41–46] covered by nm-scale granular structures, as shown in **Figure 4**. The nm-scale granular structures might have originated as particulate debris generated by laser ablation and deposited onto the silicon surface during the fs-laser irradiation process.[14] The μm-scale conical structures in the hyperdoped b-Si are about 5 μm tall and 1 μm wide at the base, with variation between individual cones. After ns-laser annealing (Figure 2) at fluences of 0.5, 1.0, and 1.5 J cm^{-2}, we observe a smoothing of

the nm-scale granular structures, while the conical structures remain intact.

Figure 5 shows the dependence of the Raman spectra on ns-laser annealing fluences. The data shows that ns-laser annealing removes the amorphous and pressure-induced polycrystalline silicon phases,[47,48] which can interfere with carrier transport, electrical rectification, and intermediate band formation.[49–57] The amount of amorphous silicon shown in the Raman spectra decreases as the annealing fluence is increased. The different contributions in the Raman spectrum require the post-processing analysis of the data to determine the centered peaks. In this case, we detect a peak centered at 520 cm^{-1}, assigned to
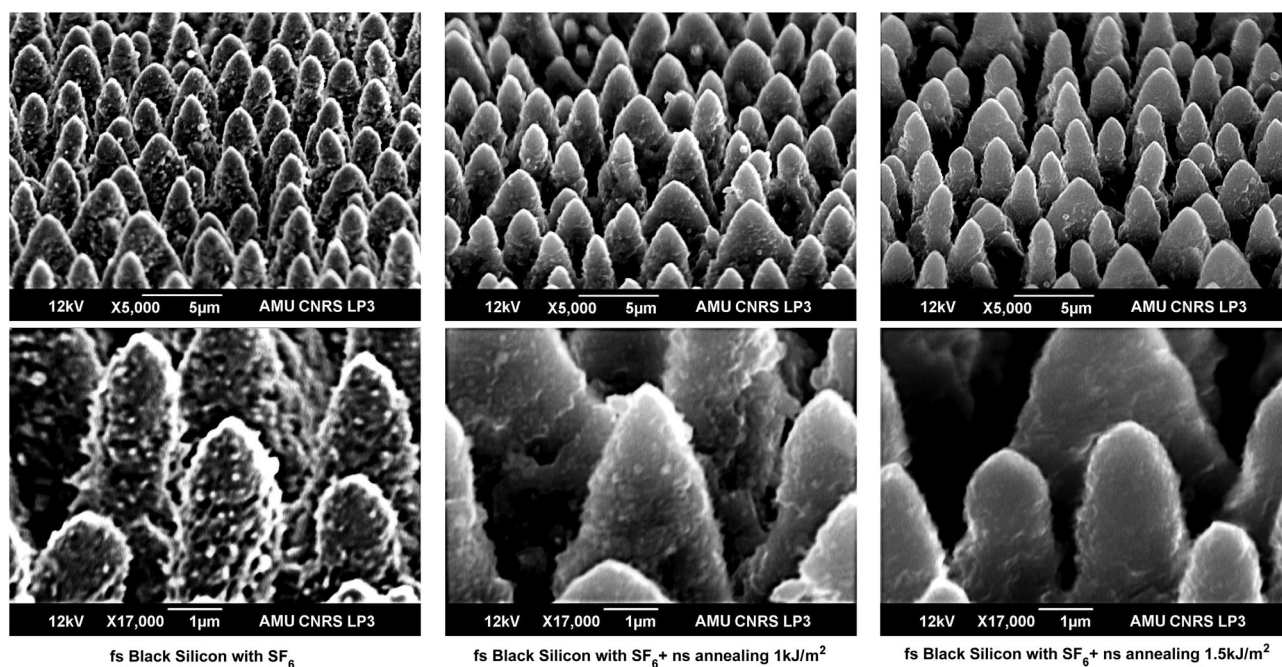

Figure 4. Hyperdoped b-Si (fabricated with fs-laser at 5 kJ m^{-2}) with nm-scale granular structures overlying conical structures about 5 μm in height and 1 μm in width (SEM tilt 45°, no foreshortening correction), without ns-laser annealing (left) and after annealing at 1 J cm^{-2} (center), and 1.5 J cm^{-2} (right). Ns-laser annealing causes smoothing of the nm-scale granular structures, while keeping the μm-scale conical structures intact.
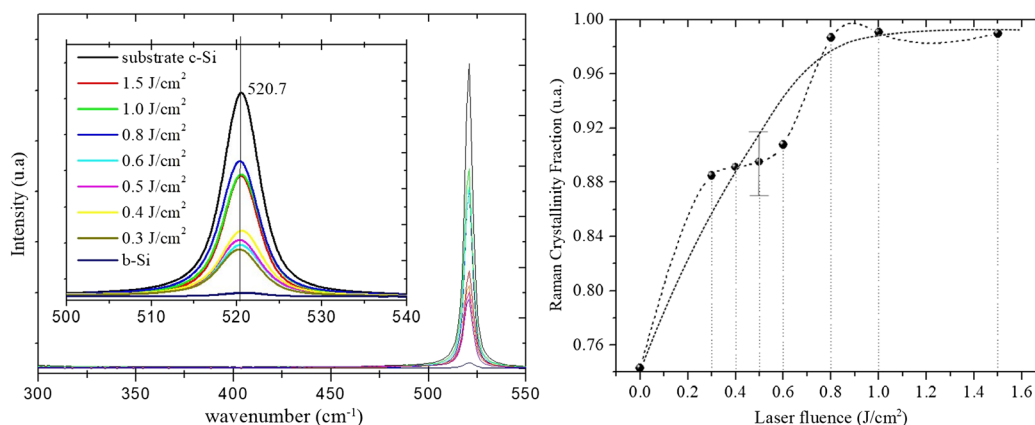
Figure 5. Raman spectra acquired at different laser annealing fluences in b-Si (left) and the corresponding fluence dependence of the crystalline fraction after annealing (right).
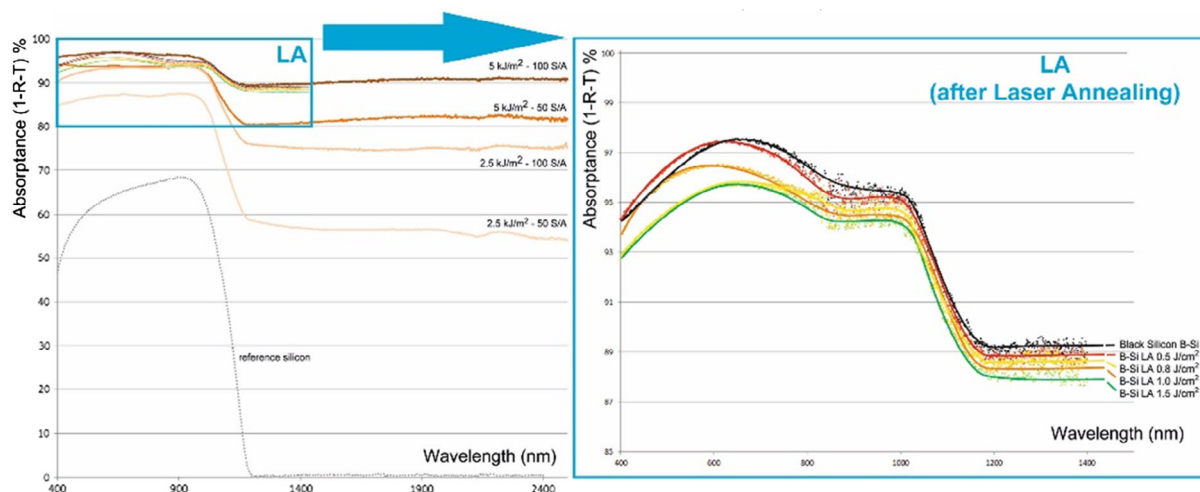
Figure 6. Left: Optical absorptance of b-Si created at different fs laser conditions (2.5–5 kJ m^{-2}, 50–100 shots per area). Right: Absorptance of the b-Si (fs irradiation at 5 kJ m^{-2}, 100 shots per area) before and after ns-laser annealing (0.5–1.5 J cm^{-2}). The absorptance decreases but remains above 93% in the visible range and above 87% in the NIR range.

the TO phonon scattering of c-Si, whereas the amorphous band appears around 480 cm^{-1}, additional peaks centered in 515 cm^{-1}, assigned to the TO phonon scattering of poly-Si which is mainly attributed to grain boundaries effects, are also considered. We determined the crystalline fraction from a deconvolution method of the Raman spectra.[58] Above 1.0 J cm^{-2}, the crystalline fraction is close to unity, indicating a nearly monocrystalline surface layer with nearly undetectable amounts of amorphous silicon.

The elimination of the amorphous and pressure-induced silicon phases after ns-laser annealing has also been confirmed in prior work using cross-sectional BF-TEM with enhanced diffraction contrast and selected area diffraction (SAD).[32]

We also analyzed the optical absorptance in the visible and near-IR of the hyperdoped b-Si samples using a spectrophotometer with an integrating sphere (**Figure 6**). The sub-bandgap absorption is reduced by about 1% by the annealing.

The observed decrease can be attributed to partial deactivation of the dopants with increasing ns-laser annealing fluence. However, even after annealing with a fluence of 1.5 J cm^{-2}, the absorptance remains around 90% in the 1–2.4 μm wavelength range. We also observe a slight decrease in visible absorption, which is probably due to the smoothening of the nanoscale roughness of the b-Si. In the wavelength range of 0.4–1 μm, the visible absorption remains above 93%.

We finally tested an IBC solar cell under visible and infrared illumination. All electrical measurements were performed with environmental temperature and humidity control under darkness, visible light, and visible plus infrared light, respectively.

The samples were illuminated in the visible with a xenon lamp with a resulting power density on the sample (1 kW m^{-2}) close to standard air mass 1.5 (AM 1.5). For IR illumination, we added a small 4.5 mW CW laser ($\lambda = 1550$ nm). The resulting IR power density was 300 mW cm^{-2} under the laser spot, corresponding to an average of 1.1 mW cm^{-2}, overall 4 cm^2 cell. Typical electrical measurements are presented in **Figure 7**. The overall efficiency is quite low, but sufficient to demonstrate a significant improvement in the infrared.

As expected, the reference c-Si cell, which was fabricated with the same processing steps for the back side (IBC with no texturization on the front side), does not exhibit additional signal when illuminated with infrared light. The black silicon (IBC b-Si) cell produces more energy in the visible due to the texturization, and its output also increases when adding infrared illumination due to dopant-mediated conversion of sub-bandgap light. The photoconversion efficiency is increased for the laser-annealed b-Si, presumably due to an increase in crystallinity and a decrease in recombination in the surface layer. Without optimization of the cell or application of a passivation layer, the efficiency of the laser-doped b-Si cell is low ($\eta = 7.6$–8.5%). However, this value is 20–30% higher than silicon reference cells ($\eta = 6.4$%).

The open-circuit voltages are quite high: 610–680 mV. These results, which are summarized in **Table 1**, could be further improved by optimizing the electrode design and passivating the surface using atomic layer deposition.[59]
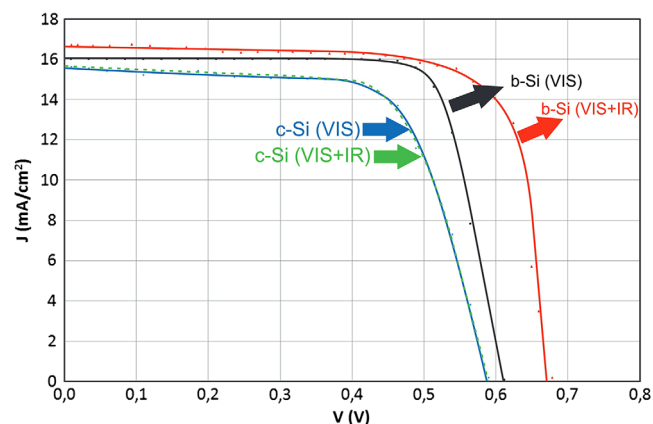
Figure 7. J–V curves under visible (VIS) and visible + infrared (VIS + IR) illumination for reference silicon (c-Si) and b-Si obtained with fs laser texturing at 5 kJ m^{-2}, 100 shots per area, 100 Torr SF$_6$ + ns-laser annealing 1 J cm^{-2}.

Table 1. PV measurements for a reference solar cell (c-Si) and black silicon solar cell (b-Si), both illuminated with visible light and visible + IR light (V_{oc}: open circuit voltage; J_{sc}: current density, 4 cm^2 cell area; FF: fill factor; η: efficiency).

Sample	Illumination	V_{oc} [mV]	J_{sc} [mA cm^{-2}]	FF	η [%]	Gain
c-Si	Visible	590	15.5	0.69	6.4	Reference
c-Si	Visible + IR	590	15.5	0.69	6.4	+0%
b-Si	Visible	612	16.0	0.78	7.6	+19%
b-Si	Visible + IR	678	16.5	0.75	8.5	+33%

Nonradiative carrier recombination, in the bulk and the interfaces, together with presence of shunt resistance contribute to the loss in photogenerated carriers. Not surprisingly, we find that the device shows poor values of efficiency.

Table 1 shows the significant gain in photoconversion efficiency using infrared light that can be obtained in a passive silicon device. The measured PV efficiency we obtained is still modest and requires further optimization, but the results nonetheless show that a laser-doped PV cell can convert sub-bandgap photons to current without decreasing the open-circuit voltage, therefore opening new prospects for achieving enhanced photoconversion efficiencies in silicon-based solar cells.[15,19,21]

4. Conclusion

The results presented in this article show that a silicon solar cell can transform infrared light into electrical energy, thanks to a combination of femtosecond laser hyperdoping and texturing followed by a nanosecond laser annealing. Preliminary results show enhanced photoconversion efficiencies of the laser-doped b-Si solar cells of 20–30% relative to c-Si reference cells. We believe the increased efficiency is due to a reduction in surface recombination from laser annealing. Higher efficiencies can be expected in the future by improving the carrier lifetime, reducing series resistance of the rear metallization grid and improving surface passivation and contact quality.

These results present new hope for intermediate band PVs, achievable through a simple, scalable processing technique. The crystallinity of the b-Si structure is restored permitting adapt this technology to the existing c-Si solar cells by improving the Si bandgap leading to an increase of the efficiency two percentual points. Although the current of the cells is still relatively low due to the lack of passivation and poor contacts which limiting the overall efficiency, several tests comparing the conversion parameters like V_{oc}, J_{sc}, and efficiency reveal the ability of the solar cell to absorb IR radiation, thanks to the post-laser annealing of the doped b-Si surface.

5. Methods

5.1. B-Si Fabrication

b-Si was created on 2×2 cm^2 silicon wafers using femtosecond laser irradiation in the presence of SF$_6$, as described in previous studies.[17,20,21]

5.2. NS-Laser Annealing Method

Nanosecond laser pulses were generated by ArF (Coherent LPX Pro 220, 193 nm, 15 ns, 250 mJ@ 100 Hz) at 100 Hz and scanned across the b-Si surface in ambient air for annealing. The ns-laser pulse fluence was controlled by reflecting a portion of the beam off a quartz window to decrease the fluence. The pulses were passed through a metal mask with a 3.0×1.0 mm^2 square opening to improve the uniformity of the pulse intensity profile, resulting in uniform pulses with fluences of 0.2–2.0 J cm^{-2}.

5.3. Interdigitated Contact Formation

The interdigitated pattern was created by a two-step LFC technique; this process consists in irradiating an Al foil (10 μm thick) covered with a spin-on-dopant (SOD) with the doping source of interest (phosphorous and boron for p-doping and n-doping, respectively), and melt this metal into the silicon substrate for creating an ohmic and highly doped contact in a single laser step. We used an excimer laser (same as the laser annealing) to melt the Al trough the Si wafer, creating the pattern electrodes, the p-region, and n-region with the same lateral dimension (1.2 mm wide). We used an interdigitated pattern with 7 p-doped strips and 7 n-doped strips with a cell area of 4 cm^2. In this IBC configuration, the metal contacts are located at the back surface of the cell, eliminating the shadowing of the front surface and the deposition of metal on a very rough surface. Another advantage of these laser-fabricated solar cells is that they do not require the extensive use of chemicals (alkaline or acid solution) and DI water, commonly used in the PV industry.

5.4. Characterization (SEM, TEM, e$^-$ Diffraction, Raman, Spectrophotometry, J–V Curves)

SEM: Morphological characterization was made using a SEM (JEOL JSM 6390). All the samples were imaged at an angle of 45° with the same acceleration voltage (12 kV) and working distance (10 mm), without foreshortening correction.

5.4.1. TEM and e-Diffraction: as Described in Franta et al.[32]

Raman: A Raman spectrometer (Jobin Yvon T64000) was used to evaluate the crystallinity of the hyperdoped b-Si surface. The excitation laser source was an argon laser (Coherent INNOVA 300) with wavelength and spot diameter are 514.4 nm and 1.5 μm, respectively. The power of the argon laser was limited to 2 mW for all the measurements to avoid any induced crystallization of analyzed samples. A peak centered at ≈520 cm^{-1}, corresponding to the transverse optical phonon scattering mode of c-Si,[20,23] is observed with an intensity increasing with the laser annealing fluence. The Raman crystalline fraction ϕ_c was evaluated after standard deconvolution of the Raman spectra.[58]

Spectrophotometry: Optical absorptance of the hyperdoped b-Si samples was analyzed using a spectrophotometer with an integrating sphere (Hitachi U-4100 and U-4001). Reflectance (R) and transmittance (T) spectra were acquired by illuminating the sample through a rectangular area (6×2 mm^2) in the

spectral range of 400–2400 nm, and the optical absorptance A was deduced from these measurements ($A = 1 - (R + T)$).

J–V Curves: J–V curves were measured using a Keithley Sourcemeter 2636 model. All measurements were performed with environmental temperature and humidity control, under darkness, visible and visible +IR light. The samples were illuminated in the visible with a Xenon lamp with a resulting power density on the sample ($1\,\text{kW m}^{-2}$) close to standard air mass 1.5 (AM1.5). We added for IR illumination a small 4.5 mW CW laser ($l = 1550$ nm). The resulting IR power density was $0.3\,\text{W cm}^{-2}$ under the laser spot, corresponding to an average of $1.1\,\text{mW cm}^{-2}$ on the whole cell (4 cm^2).

Conflict of Interest

The authors declare no conflict of interest.

Data Availability Statement

The data that support the findings of this study are openly available in MI Sanchez Aniorte Publications at https://data.mendeley.com/datasets/p4wxpp7fp4/1.

[1] P. K. Nayak, S. Mahesh, H. J. Snaith, D. Cahen, *Nat Rev Mater* **2019**, *4*, 269.

[2] G. M. Wilson, M. Al-Jassim, W. K. Metzger, S. W. Glunz, P. Verlinden, G. Xiong, L. M. Mansfield, B. J. Stanbery, K. Zhu, Y. Yan, J. J. Berry, A. J. Ptak, F. Dimroth, B. M. Kayes, A. C. Tamboli, R. Peibst, K. Catchpole, M. O. Reese, C. S. Klinga, P. Denholm, M. Morjaria, M. G. Deceglie, J. M. Freeman, M. A. Mikofski, D. C. Jordan, *J. Phys. D: Appl. Phys.* **2020**, *53* 493001.

[3] M. A. Green, E. D. Dunlop, J. Hohl-Ebinger, M. Yoshita, N. Kopidakis, A. W. Y. Ho-Baillie, **2020**, *28*, 3.

[4] K. Yoshikawa, H. Kawasaki, W. Yoshida, T. Irie, K. Konishi, K. Nakano, T. Uto, D. Adachi, M. Kanematsu, H. Uzu, K. Yamamoto, *Nat. Energy* **2017**, *2*, 17032.

[5] A. Richter, M. Hermle, S. W. Glunz, *IEEE J. Photovolt.* **2013**, *3*, 1184.

[6] D. Joseph, S. Senthilarasu, T. K. Mallick, *Renew. Energy* **2019**, *132*, 186.

[7] M. M. Lee, J. Teuscher, T. Miyasaka, T. N. Murakami, H. J. Snaith, *Science* **2012**, *338*, 643.

[8] B. McKenna, R. C. Evans, *Adv. Mater.* **2017**, *29*, 1606491.

[9] T. Trupke, M. A. Green, *J. Appl. Phys.* **2002**, *92*, 4117.

[10] T. Trupke, M. A. Green, *J. Appl. Phys.* **2002**, *92*, 1668.

[11] B. S. Shalav, *Sol. Energy Mater. Sol. Cells* **2007**, *91*, 835.

[12] K. Yu, J. Ouyang, Y. Zhang, H. T. Tung, S. Lin, R. A. L. Nagelkerke, D. Kingston, X. Wu, D. M. Leek, D. Wilkinson, C. Li, I. G. Chen, Y. Tao, *ACS Appl. Mater. Interfaces* **2011**, *3*, 1511.

[13] J. Lv, T. Zhang, P. Zhang, Y. Zhao, S. Li, *Nanoscale Res. Lett.* **2018**, *13*, 110.

[14] J. P. Mailoa, A. J. Akey, C. B. Simmons, D. Hutchinson, J. Mathews, J. T. Sullivan, D. Recht, M. T. Winkler, J. S. Williams, J. M. Warrender, P. D. Persans, M. J. Aziz, T. Buonassisi, *Nat. Commun.* **2014**, *5*, 3011.

[15] a) J. P. Mailoa, A. J. Akey, C. B. Simmons, D. Hutchinson, J. Mathews, J. T. Sullivan, D. Recht, M. T. Winkler, J. S. Williams, J. M. Warrender, P. D. Persans, M. J. Aziz, T. Buonassisi, *Nat. Commun.* **2014**, *5*, 3011; b) A. Luque, A. Martí, C. Stanley, *Nat. Photonics* **2012**, *6*, 146.

[16] E. Ertekin, M. T. Winkler, D. Recht, A. J. Said, M. J. Aziz, T. Buonassisi, J. C. Grossman, *Phys. Rev. Lett.* **2012**, *108*, 026401.

[17] C. B. Simmons, A. J. Akey, J. P. Mailoa, D. Recht, M. J. Aziz, T. Buonassisi, *Adv. Funct. Mater.* **2014**, *24*, 2852.

[18] M.-J. Sher, E. Mazur, *Appl. Phys. Lett.* **2014**, *105*, 032103.

[19] A. Luque, A. Martí, *Phys. Rev. Lett.* **1997**, *78*, 5014.

[20] K. M. Guenther, T. Gimpel, J. W. Tomm, S. Winter, A. Ruibys, S. Kontermann, W. Schade, *Appl. Phys. Lett.* **2014**, *104*, 042107.

[21] T. Her, R. J. Finlay, C. Wu, S. Deliwala, E. Mazur, *Appl. Phys. Lett.* **1998**, *73*, 1673.

[22] C. H. Crouch, J. E. Carey, J. M. Warrender, M. J. Aziz, E. Mazur, F. Y. Génin, *Appl. Phys. Lett.* **2004**, *84*, 1850.

[23] C. H. Crouch, J. E. Carey, M. Shen, E. Mazur, F. Y. Génin, *Appl. Phys. A* **2004**, *79*, 1635.

[24] M. A. Sheehy, L. Winston, J. E. Carey, C. M. Friend, E. Mazur, *Chem. Mater.* **2005**, *17*, 3582.

[25] K. N. Barada, C. G. Mool, W. K. Kurt, *Nanotechnology* **2007**, *18*, 195302.

[26] T. Sarnet, M. Halbwax, R. Torres, P. Delaporte, M. Sentis, S. Martinuzzi, V. Vervisch, F. Torregrosa, H. Etienne, L. Roux, S. Bastide, *Proc. SPIE* **2008**, *6881*, 688119-2.

[27] T. Sarnet, T. J.-Y. Derrien, R. Torres, Ph. Delaporte, F. Torregrosa, M.-J. Sher, Y.-T. Lin, B. Franta, G. Deng, E. Mazur, *J. Optoelectron. Adv. M.* **2010**, *12*, 621.

[28] T. J.-Y. Derrien, R. Torres, T. Sarnet, M. Sentis, T. Itina, *Appl. Surf. Sci.* **2012**, *258*, 9487.

[29] R. R. Gattass, E. Mazur, *Nat. Photonics* **2008**, *2*, 219.

[30] S. Y. Chou, C. Keimel, J. Gu, *Nature* **2002**, *417*, 835.

[31] H. Savin, P. Repo, G. von Gastrow, P. Ortega, E. Calle, M. Garín, R. Alcubilla, *Nat. Nanotechnol.* **2015**, *10*, 624.

[32] B. Franta, D. Pastor, H. H. Gandhi, P. H. Rekemeyer, S. Gradečak, M. J. Aziz, E. Mazur, *J. Appl. Phys.* **2015**, *118*, 225303.

[33] M. O. Thompson, J. W. Mayer, A. G. Cullis, H. C. Webber, N. G. Chew, J. M. Poate, D. C. Jacobson, *Phys. Rev. Lett.* **1983**, *50*, 896.

[34] J. Förster, H. Vogt, in *Proc. COMSOL* **2011**.

[35] J. Narayan, C. W. White, M. J. Aziz, B. Stritzker, A. Walthuis, *J. Appl. Phys.* **1985**, *57*, 564.

[36] M. Halbwax, T. Sarnet, Ph. Delaporte, M. Sentis, H. Etienne, F. Torregrosa, V. Vervisch, I. Perichaud, S. Martinuzzi, *Thin Solid Films* **2008**, *516*, 6791.

[37] P. Ortega, A. Orpella, I. Martín, M. Colina, G. López, C. Voz, M. I. Sánchez, C. Molpeceres, R. Alcubilla, *Progr. Photovolt. Res. Appl.* **2012**, *20*, 173.

[38] P. Ortega, *Prog. Photovolt. Res. Appl.* **2015**, *23*, 1448.

[39] E. Schneiderlöchner, R. Preu, R. Lüderman, S. W. Glunz, *Progr. Photovolt.* **2002**, *10*, 29.

[40] T. Röder, P. Grabitz, S. Eisele, C. Wagner, J. R. Kohler, J. H. Werner, in *34th Photovoltaic Specialists Conf. (PVSC)*, IEEE, Piscataway, NJ **2009**; https://doi.org/10.1109/PVSC.2009.5411149.

[41] J. Bonse, J. Krüger, S. Höhm, A. Rosenfeld, *J. Laser Appl.* **2012**, *24* 042006.

[42] J. E. Sipe, J. F. Young, J. S. Preston, H. M. van Driel, *I. Theory. Phys. Rev. B* **1983**, *27* 1141.

[43] G. Obara, H. Shimizu, T. Enami, E. Mazur, M. Terakawa, M. Obara, *Opt. Express* **2013**, *21*, 26323.

[44] A. Y. Vorobyev, C. Guo, *Opt. Express* **2011**, *19*, A1031.

[45] B. K. Nayak, V. V. Iyengar, M. C. Gupta, *Prog. Photovolt.* **2011**, *19*, 631.

[46] Y. F. Huang, S. Chattopadhyay, Y.-J. Jen, C.-Y. Peng, T.-A. Liu, Y.-K. Hsu, C.-L. Pan, H.-C. Lo, C.-H. Hsu, Y.-H. Chang, C.-S. Lee, K.-H. Chen, L.-C. Chen, *Nat. Nanotech.* **2007**, *2*, 770.

[47] M. J. Smith, Y.-T. Lin, M.-J. Sher, M. T. Winkler, E. Mazur, S. Gradečak, *J. Appl. Phys.* **2011**, *110*, 053524.

[48] M. J. Smith, M.-J. Sher, B. Franta, Y.-T. Lin, E. Mazur, S. Gradečak, *J. Appl. Phys.* **2012**, *112*, 083518.

[49] J. Bonse, *Appl. Phys. A* **2006**, *84*, 63.

[50] M. J. Smith, M.-J. Sher, B. Franta, Y.-T. Lin, E. Mazur, S. Gradečak, *Appl. Phys. A* **2014**, *114*, 1009.

[51] C. B. Simmons, A. J. Akey, J. J. Krich, J. T. Sullivan, D. Recht, M. J. Aziz, T. Buonassisi, *J. Appl. Phys.* **2013**, *114*, 243514.

[52] M. J. Sher, N. M. Mangan, M. J. Smith, Y.-T. Lin, S. Marbach, T. M. Schneider, S. Gradečak, M. P. Brenner, E. Mazur, *J. Appl. Phys.* **2015**, *117*, 125301.

[53] K.-M. Guenther, T. Gimpel, S. Kontermann, W. Schade, *Appl. Phys. Lett.* **2013**, *102*, 202104.

[54] N. H. Nickel, *Laser Crystallization of Silicon*, Elsevier **2003**.

[55] P. Lorazo, L. J. Lewis, M. Meunier, *Phys. Rev. B* **2006**, *73*, 134108.

[56] M. J. Sher, C. B. Simmons, J. J. Krich, A. J. Akey, M. T. Winkler, D. Recht, T. Buonassisi, M. J. Aziz, A. M. Lindenberg, *Appl. Phys. Lett.* **2014**, *105*, 053905.

[57] J. Oh, H.-C. Yuan, H. M. Branz, *Nature Nanotech.* **2012**, *7*, 743.

[58] A. T. Voutsas, M. K. Hatalis, J. Boyce, A. Chiang, *J. Appl. Phys.* **1995**, *78*, 6999.

[59] W. Niu, X. Li, S. K. Karuturi, D. W. Fam, H. Fan, S. Shrestha, L. H. Wong, A. I. Y. Tok, *Nanotechnology* **2015**, *26*, 064001.

2000550 (8 of 8)